

# Three-body properties of low-lying $^{12}\text{Be}$ resonances

E. Garrido<sup>1</sup>, A.S. Jensen<sup>2</sup>, D. V. Fedorov<sup>2</sup>, J. G. Johansen<sup>2</sup>

<sup>1</sup> *Instituto de Estructura de la Materia, IEM-CSIC, Serrano 123, E-28006 Madrid, Spain and*

<sup>2</sup> *Department of Physics and Astronomy, Aarhus University, DK-8000 Aarhus C, Denmark*

(Dated: August 6, 2018)

We compute the three-body structure of the lowest resonances of  $^{12}\text{Be}$  considered as two neutrons around an inert  $^{10}\text{Be}$  core. This is an extension of the bound state calculations of  $^{12}\text{Be}$  into the continuum spectrum. We investigate the lowest resonances of angular momenta and parities,  $0^\pm$ ,  $1^-$  and  $2^+$ . Surprisingly enough, they all are naturally occurring in the three-body model. We calculate bulk structure dominated by small distance properties as well as decays determined by the asymptotic large-distance structure. Both  $0^+$  and  $2^+$  have two-body  $^{10}\text{Be}$ -neutron  $d$ -wave structure, while  $1^-$  has an even mixture of  $p$  and  $d$ -waves. The corresponding relative neutron-neutron partial waves are distributed among  $s$ ,  $p$ , and  $d$ -waves. The branching ratios show different mixtures of one-neutron emission, three-body direct, and sequential decays. We argue for spin and parities,  $0^+$ ,  $1^-$  and  $2^+$ , to the resonances at 0.89, 2.03, 5.13, respectively. The computed structures are in agreement with existing reaction measurements.

PACS numbers: 21.45.-v, 21.60.Gx, 25.70.Ef, 27.20.+n

## I. INTRODUCTION

Cluster and halo states in light nuclei have been studied for several decades [1–4]. These structures are to a large extent decoupled from more complicated many-body states since they occupy essentially separate parts of the Hilbert space. The descriptions of these cluster structures are usually in terms of few-body correlations, i.e., two or three almost inert clusters interacting through effective potentials. These constituent clusters are themselves nuclear systems. Thus, the full nuclear many-body system is described by separate relative and internal cluster degrees of freedom. The first and most important step for halo states is then to freeze the internal motion in a given structure, and solve the remaining relative motion.

Bound states are only a small part of the possible quantum structures of a given many-body system. Among the infinitely many continuum states one can find resonances, still by definition in the continuum, but that can be understood as a discrete continuation of the set of bound state structures. As the excitation energy increases it is expected that the underlying assumption of uncoupled internal and relative cluster motion becomes increasingly violated. However, a number of low-lying many-body resonances in light nuclei can still be well described as cluster structures even when they appear in the continuum. Prominent examples are found in stable nuclei like  $^{12}\text{C}$  and  $^9\text{Be}$  [5–13], but even ground states like in  $^6\text{Be}$  [14–17] and  $^{10}\text{Li}$  [18–20] may appear as resonances.

A number of beta unstable light nuclei exhibit particle stable bound cluster states, f.ex.  $^{11}\text{Li}$  [3, 21],  $^{17}\text{Ne}$  [22–24] and  $^{12}\text{Be}$  [25–29]. In many cases the bound states are well established, but very often their particle unstable spectrum is much less known due to practical experimental difficulties. The excited  $1^-$  state in  $^{11}\text{Li}$  is a clear example [30–33].

An interesting point is that very often the neutron dripline has states of a unique structure. In particular,

$^{11}\text{Be}$  is a nucleus with two bound states, both with a two-body halo structure. The ground state of  $^{12}\text{Be}$  is rather well bound but three halo states appear as excited states, and  $^{13}\text{Be}$  is particle unbound, whereas  $^{14}\text{Be}$  has one particle-bound state [34, 35]. The complicated dripline structure for the Be-isotopes is primarily due to the second  $s$ -state intruder and eventual inversion with the  $p$ -state in  $^{11}\text{Be}$  [36]. Correlations of the valence neutrons in a larger space result in unusually many bound states compared to other light dripline nuclei.

Beside the bound (halo) states in  $^{12}\text{Be}$ , a  $0^-$ -state has been suggested [37, 38], looked for in experiments, but so far not found as a bound state. The structure of the effective potentials in the three-body problem of  $^{12}\text{Be}$  ( $^{10}\text{Be}+n+n$ ) is complicated and suggesting more excited states than the known bound states. The one-neutron threshold is lower than the two-neutron threshold, implying that a resonance of one-body nature could appear between the two thresholds. Its structure would then at large distance have to be one neutron far away from  $^{11}\text{Be}$  either in the ground or the excited state.

There has been very little experimental investigations of the resonances in  $^{12}\text{Be}$ . Two resonances were seen in a  $^{10}\text{Be}(t,p)^{12}\text{Be}$  experiment by Fortune et al. [39], which was later confirmed by Bohlen et al. [40]. The energy and width were measured, and set to 0.89 MeV and 2.03 MeV above the two-neutron threshold. The strong population of the resonances in a two neutron transfer indicates a natural parity ( $0^+, 1^-, 2^+, \dots$ ), and tentatively quantum numbers were given from DWBA calculations.

It seems to be very appropriate to extend the theoretical bound state study of  $^{12}\text{Be}$  to the continuum. The purpose of the present paper is to investigate the low-lying resonance structure of  $^{12}\text{Be}$ . In section II we very briefly sketch the method, the previously applied effective  $^{10}\text{Be}$ -neutron interactions, and the adiabatic  $^{12}\text{Be}$  potentials. In section III, we present resonance energies and their quantum numbers. In section IV, we discuss

the resonance structures. In section V, we discuss the production and decay modes of the resonances and compare our results with known experimental data. Finally, in section VI we give a short summary and the corresponding conclusions.

## II. BASIC INGREDIENTS

The theoretical framework has been previously well described and successfully applied [27]. We only briefly sketch to define notation and interactions. The resulting adiabatic potentials are the basic ingredients in the subsequent calculations.

### A. Method and interactions

We use the adiabatic hyperspherical expansion method to calculate the three-body properties of the system in question, that is  $^{12}\text{Be}$  ( $^{10}\text{Be}+n+n$ ). This method strictly deals with three entities treated as point-like particles interacting pairwise with each other [41]. The Faddeev equations are first formulated in hyperspherical coordinates which consists of the hyperradius,  $\rho$ , and five angles collectively named  $\Omega$ .

Assuming that the two-body interactions are known, we can solve the angular part of the Faddeev equations for fixed hyperradius. Due to the restriction of finite intervals for all five angular coordinates the eigenvalue spectrum is discrete, although in principle with infinitely many elements. The angular solutions form a complete set which is exploited as a basis for expansion of the total wave function. This provides finally a coupled set of one-dimensional hyperradial equations. The details of the method are discussed in [41].

Bound states are solutions to the radial equation with an exponentially falling radial large-distance behavior. Resonances are solutions to the same hyperradial equations but with boundary conditions corresponding to only outgoing waves. We apply the complex rotation method on the hyperspherical coordinates, that is only the hyperradius is scaled by  $\exp(i\theta)$  [42]. The resonance boundary conditions are then transformed to an exponential fall-off, precisely as the bound states, provided the rotation angle,  $\theta$ , exceeds  $\arctan(\Gamma/2E_R)$ , which is the value corresponding to rotation of the real-energy axis to the position of the resonance, ( $E_R, E_I = -\Gamma/2$ ). We have here denoted the real and imaginary values of the resonance energy by  $E_R$  and  $E_I$ .

The two-body interactions between the two neutrons and between neutron and  $^{10}\text{Be}$  can be chosen through different criteria. They are all related to the corresponding two-body properties of bound states and/or resonances. The crucial pieces are the  $s$ ,  $p$ , and  $d$ -wave interactions. The neutron-neutron interaction from [27] reproduces low-energy scattering properties for the different partial waves. For neutron- $^{10}\text{Be}$ , we choose effec-

tive potentials for each set of quantum numbers such that the lowest computed energy reproduces the bound state or resonance energy.

In particular, we use the interaction labeled I in [27], where the central and spin-orbit radial potentials are assumed to have a gaussian shape. The range of this interaction for all the partial waves is taken equal to 3.5 fm, that is the sum of the rms radius of the core and the radius of the neutron. For  $s$ -waves the strength is fixed to fit the experimental neutron separation energy of the  $1/2^+$ -state in  $^{11}\text{Be}$  ( $-0.504$  MeV). For  $p$ -waves the two free parameters (central and spin-orbit strengths) are adjusted to reproduce the experimental neutron separation energy of the  $1/2^-$ -state in  $^{11}\text{Be}$  ( $-0.184$  MeV), and simultaneously push up the  $3/2^-$  state, which is forbidden by the Pauli principle, since it is occupied by the four neutrons in the  $^{10}\text{Be}$  core. For the  $d$ -states it is well established that  $^{11}\text{Be}$  has a  $5/2^+$  resonance at 1.28 MeV (energy above threshold), and the most likely candidate as spin-orbit partner of the  $5/2^+$  state is the known  $3/2^+$ -resonance at 2.90 MeV (above threshold) [43]. Simultaneous matching of these two resonances (and the corresponding widths) leads to central and spin-orbit radial potentials for  $d$ -waves made as a sum of two gaussians. Further details about the interaction are discussed in [27].

Typically, in a three-body calculation an effective three-body force is introduced in the coupled set of radial equations in order to fine tune the properties of the three-body system [41]. This potential can be understood as the way to take care of all those effects that go beyond the two-body interactions. In our calculations we have used a gaussian three-body force, whose range has been taken equal to 4.25 fm, that is the hyperradius corresponding to a  $^{10}\text{Be}$ -core and two neutrons touching each other. The strength of the gaussian is used to adjust the energy of the computed resonance. Once this is done, the width is determined by the potential barrier (height and thickness) at that precise energy. A change of the range in the three-body potential could affect the properties of the barrier (and therefore the width of the resonance), but a modest change produces only very modest variations of the width. This is because the strength is adjusted to maintain the energy which is the crucially important quantity determining the width. Thus the conclusions reached in this work would still hold.

### B. Adiabatic cluster potentials

The solutions to the complex rotated angular equations provide the set of complex hyperradial adiabatic potentials whose real parts are shown in Fig.1 for each of the most interesting sets of angular momentum and parity. Most of these potentials approach zero at large distances. However, several of them approach values less than or larger than zero. These asymptotic energies are two-body bound state or resonance energies correspond-

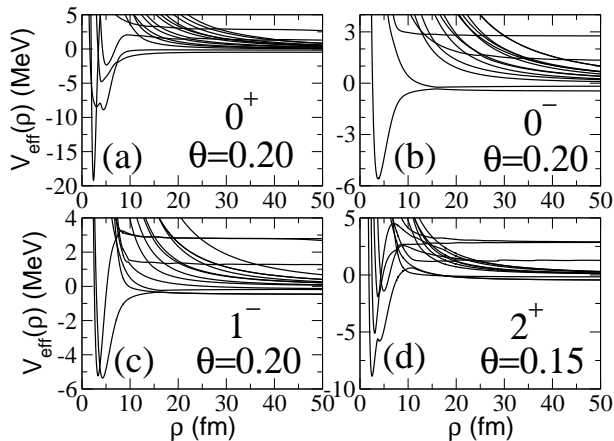


FIG. 1. Real parts of the dominating lowest-lying adiabatic potentials as functions of hyperradius for  $^{12}\text{Be}$  for total angular momentum  $J^\pi = 0^\pm, 1^-, 2^+$ . The scaling angle,  $\theta$  (in rad), is given in the figure for each  $J^\pi$ .

ing to two particles in those relative states while the third particle is far away. Below zero it must be the  $s_{1/2}$  or  $p_{1/2}$  bound states of  $^{11}\text{Be}$  at respectively  $-0.504$  MeV and  $-0.184$  MeV. Above zero it must be the  $d_{3/2}$  or  $d_{5/2}$ -resonances, respectively at  $2.90$  MeV and  $1.28$  MeV above the three-body threshold [43].

At smaller distances, all the potentials diverge towards  $+\infty$ , and at finite, but relatively small distances, a substantial amount of structure is present. The attractive pockets are responsible for structures like three-body bound states or resonances. If all potentials are repulsive at all distances, no structure can arise and all three particles would try to get as far from each other as possible.

The  $0^-$  set of potentials are the simplest as only one of the potentials exhibits some attraction. However, this level crosses, or rather avoids crossing, another purely repulsive level when  $\rho$  is about  $15$  fm. The large-distance asymptotics of these two crossing levels then correspond to the  $^{11}\text{Be}$  in the  $s_{1/2}$  or  $p_{1/2}$  bound states and the last neutron spatially far away corresponding in  $p_{1/2}$  or  $s_{1/2}$ -states with respect to the center of mass of the  $^{11}\text{Be}$  states. Only these combinations are allowed since the total angular momentum and parity,  $0^-$ , has to arise after coupling of these angular momenta. Thus, the attractive pocket seems to be mostly of  $^{11}\text{Be}(p_{1/2})$  character, since this configuration is reached by the smooth continuation of the attractive structure to large distances beyond the avoided crossing.

The  $1^-$  set of potentials are also relatively simple with only two potentials with attractive pockets where the thickest and deepest resembles the lowest  $0^-$  potential. Also for  $1^-$ , this potential avoids crossing another potential, and together they form the same large-distance asymptotic structure as the two lowest  $0^-$  potentials. The only difference is that the  $s_{1/2}$  and  $p_{1/2}$  angular

momenta now are coupled to  $1^-$ . The other potential with an attractive pocket is thinner and rather steeply increasing to “avoid crossing” a number of other potentials where the first is the purely repulsive potential ending up as the lowest at large distance. This potential therefore has a barrier, and consequently it may be able to hold a resonance. Due to the possibly complicated rearrangements of structures at crossings the decay path and resulting decay channels cannot be derived by inspection of these potentials.

Both  $0^+$  and  $2^+$  sets of potentials are much more structured. Now four potentials have attractive pockets at small distances and each has fast small-scale variation arising from crossings at these hyperradii. The two large-distance  $^{11}\text{Be}$  structures are again for both  $0^+$  and  $2^+$  found as potentials approaching  $-0.504$  MeV and  $-0.184$  MeV. For  $0^+$  the last neutron is then in  $s_{1/2}$  or  $p_{1/2}$  states relative to  $^{11}\text{Be}(s_{1/2})$  or  $^{11}\text{Be}(p_{1/2})$ . For  $2^+$ , three negative states appear at large distance with the last neutron in the  $d_{5/2}$ ,  $d_{3/2}$  or in the  $p_{3/2}$  state relative to the two bound states of  $^{11}\text{Be}$ . The complicated structures of the potentials do not allow quick predictions of occurrence of bound states or resonances and their structure or decay properties. Detailed investigations must be carried out.

### III. BOUND STATE AND RESONANCE ENERGIES

The potentials in Fig.1 are applied to the coupled set of hyperradial equations. Bound state energies are then first obtained as described in details in [27], that is the experimentally known ground state of  $0^+$ , and the excited states of  $0^+$ ,  $1^-$  and  $2^+$ . In precisely the same framework a  $0^-$  state was also found [37]. So far, this state has not been seen in experiments.

The same basic interactions that produced the adiabatic potentials in Fig.1 are also able to support resonances. They are computed by the complex scaling technique [42] as poles of the  $S$ -matrix. The precise positions cannot be reliably obtained since polarization effects are excluded beyond the two-body level, and contributions from other neglected degrees of freedom can be crucial. To mock up effects of these omissions we tune the real parts of the three-body energies to an a priori chosen value. The imaginary part, or equivalently the width of the states, then follow without further adjustment.

The attractive pocket for  $0^-$  in Fig.1 is sufficiently strong to support the bound state suggested in [37], although no experimental evidence of it has been found so far. The reason for this can be either because its population in reactions is extremely small, or it is hidden behind the other states, or it is for some reason pushed up into the continuum. We investigate consequences of the last option where both one-body ( $^{11}\text{Be} + n$ ) and two-body ( $^{10}\text{Be} + n + n$ ) continuum structures in principle are possible.

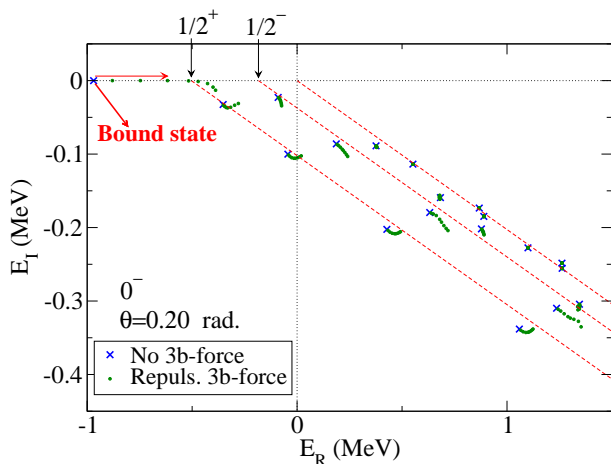


FIG. 2. (Color online) The complex scaled spectrum for  $0^-$  states in  $^{12}\text{Be}$  ( $^{10}\text{Be}+n+n$ ). The down sloping lines are the rotated one-neutron thresholds for ground and excited states of  $^{11}\text{Be}$ -neutron and the two-neutron threshold for  $^{10}\text{Be}+n+n$ . The rotation angle is 0.20 rad. The points are the discrete states computed in the continuum. The crosses have been obtained without inclusion of any three-body force. The close-lying sets are sequences of points arising from variation of the strength of the repulsive three-body interaction.

In Fig.2 we show the  $0^-$  complex energy spectrum where the repulsion of the three-body interaction is increased from zero. The spectrum with zero repulsion is shown by the crosses in the figure, where a  $0^-$  bound state appears at an energy of about  $-1$  MeV. The closed circles show the spectrum when the three-body repulsion is gradually increased. We see that the first threshold, ground state of  $^{11}\text{Be}$ , is approached when the real part of the energy corresponds to a true bound state and the imaginary part is zero. Passing the threshold allows a finite imaginary part of the energy, which very quickly increases, and very soon disappears in the rotated continuum threshold. The result is that this emerging neutron- $^{11}\text{Be}$  one-body resonance state is dissolved in this continuum. It can then stay in the continuum with a large width or continue to rotate and end up as a virtual state on another Riemann sheet with zero imaginary energy. We cannot decide with the present amount of information. In any case, we cannot move the resonance to even higher values, approaching or passing, the next two thresholds. Thus, we conclude that the  $0^-$  state is either bound, a very broad resonance structure, or a virtual state only revealing itself via an attractive potential.

In Fig.3 we show the  $1^-$  complex energy spectrum in  $^{12}\text{Be}$ . Now, together with the three down sloping lines for the one-neutron and two-neutron threshold, we also show the two lines corresponding to the rotated thresholds for the  $d_{5/2}$  and  $d_{3/2}$  resonances in  $^{11}\text{Be}$ . These two thresholds are present in the  $1^-$  states, which makes the spectrum more complicated than for the  $0^-$  states. When no three-body interaction is used, the  $1^-$  spectrum gives

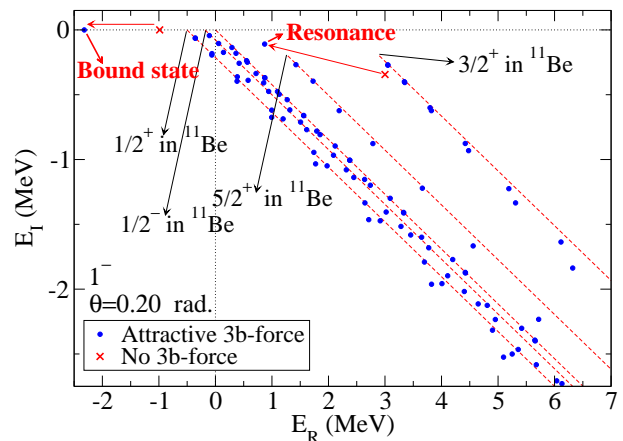


FIG. 3. (Color online) The complex scaled spectrum for the  $1^-$  states in  $^{12}\text{Be}$  ( $^{10}\text{Be}+n+n$ ). The two first down sloping lines are the rotated one-neutron thresholds for ground and excited states of  $^{11}\text{Be}$ -neutron and the third tilted line is the two-neutron threshold for  $^{10}\text{Be}+n+n$ . The last two tilted lines are the thresholds corresponding to the two  $d$ -wave resonances in  $^{11}\text{Be}$ . The rotation angle is 0.20 rad. The points are the discrete states computed in the continuum. The crosses are the bound state and the resonance obtained without inclusion of any three-body force. The closed circles have been obtained with an attractive three-body force which moves the bound state and the resonance as indicated by arrows.

rise to one bound state close to  $-1$  MeV, and to a resonance at a complex energy of  $(2.99, -0.34)$  MeV, which are indicated by the crosses in the figure. The signature of the resonance is a numerically stable and distinguishable point outside all the rotated continuum thresholds. An additional attraction, in particular the one provided by an effective three-body force, moves down the resonance towards the three-body threshold. It is then not difficult to adjust this attractive force to fit the known experimental resonance energies in  $^{12}\text{Be}$ . When adjusting the energy to 2.0 MeV the computed width is of about 0.50 MeV, clearly larger than the corresponding experimental width of 0.09 MeV given in [39]. When fitting the energy to 0.9 MeV, the computed width is of 0.22 MeV, a factor of 2 larger than the experimental width quoted in [39] for this resonance. This last spectrum is the one shown by the closed circles in Fig. 3. This size order is in general not allowing for contributions from configurations omitted in the three-body model.

In Fig.4 we show the  $0^+$  complex energy spectrum which gives rise to two bound states (only one shown in the figure). However, both the potentials in Fig.1 and the present spectrum are more complicated than those of the  $0^-$  states. The properties of the spectrum are qualitatively very similar to those described for the  $1^-$  states, but now the computed resonance energy without three-body potential is 1.97 MeV. The crosses in the figure indicate this resonance and one of the bound states. This resonance energy already matches one of the exper-

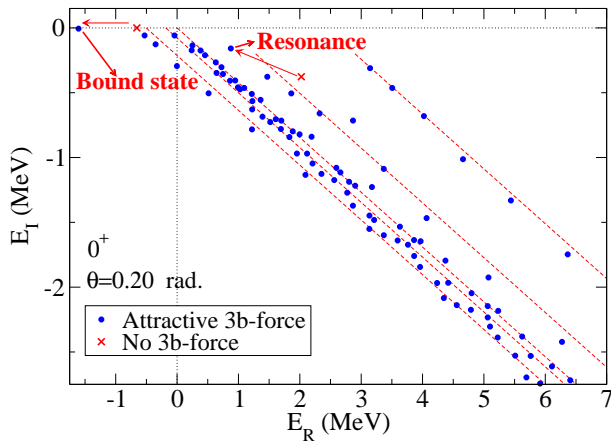


FIG. 4. (Color online) the same as Fig.3 for the  $0^+$  spectrum in  $^{12}\text{Be}$  ( $^{10}\text{Be}+n+n$ ). The down sloping lines are the same thresholds as described in Fig.3. The rotation angle is 0.20 rad. The points are the discrete states computed in the continuum. Again, the crosses are the bound state and the resonance obtained without inclusion of any three-body force, and the closed circles have been obtained with an attractive three-body force which moves the bound state and the resonance as indicated by arrows.

imental known energies, although again the computed width (0.70 MeV) is clearly larger than the experimental one. Moving this resonance down by use of an attractive three-body potential it is also possible to place the resonance at 0.89 MeV, but again the computed width of 0.32 MeV is clearly larger than the experimental one, now a factor of three larger. The corresponding full spectrum is shown by the closed circles in the figure.

In Fig.5 we show the  $2^+$  complex energy spectrum which gives rise to one bound state. Again, we notice that both the potentials in Fig.1 and the present spectrum are more complicated than those of the  $0^-$  states. The properties of the spectrum are again qualitatively very similar to those of the  $0^+$  and  $1^-$  states. The resonance position without three-body potential is now around (5.36, -0.60) MeV (crosses in the figure). However, in this case the attractive three-body potential now has to be exceedingly strong to move the position down to 0.9 MeV. For this reason, our calculation excludes the assignment of the spin and parity  $2^+$  for the resonance experimentally known to be around this energy. Even more, a moderate strength would place the resonance not much lower than about 2.8 MeV, and having a width of 0.7 MeV. This is the spectrum shown by the solid circles in the figure. This computed resonance could at most be compatible with the second reported measured resonance of the same energy with a much smaller width of about 0.086 MeV [39], but more likely it would be more suitable for a higher lying resonance, a possible candidate were observed at 5.13 MeV by Bohlen et al. [40].

A summary with the computed energies and widths for the different resonances is given in table I. The sec-

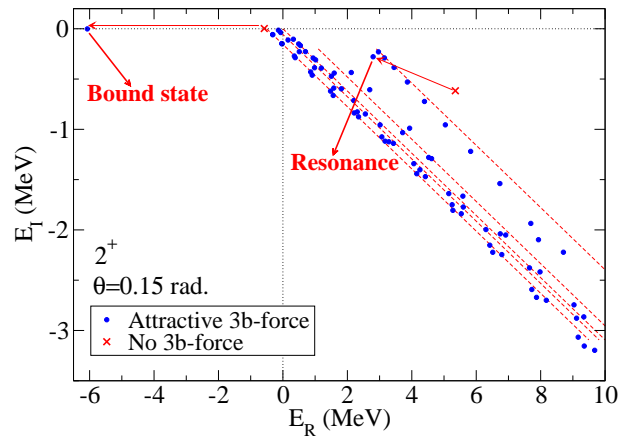


FIG. 5. (Color online) the same as Fig.3 for the  $2^+$  spectrum in  $^{12}\text{Be}$  ( $^{10}\text{Be}+n+n$ ). The down sloping lines are the same thresholds as described in Fig.3, although now the rotation angle is 0.15 rad. The points are the discrete states computed in the continuum. Again, the crosses are the bound state and the resonance obtained without inclusion of any three-body force, and the closed circles have been obtained with an attractive three-body force which moves the bound state and the resonance as indicated by arrows.

TABLE I. Computed energies and widths (both in MeV) for different angular momenta and parity states in  $^{12}\text{Be}$ . The second column is the result without inclusion of a three-body force. In the third and fourth columns a three-body force has been included to fit the computed energy to the ones known experimentally [39, 40].

	No 3b-force	with 3b-force	with 3b-force
	$(E_R, \Gamma)$	$(E_R, \Gamma)$	$(E_R, \Gamma)$
$1^-$	(2.99, 0.68)	(0.89, 0.22)	(2.03, 0.50)
$0^+$	(1.97, 0.70)	(0.89, 0.32)	(2.03, 0.84)
$2^+$	(5.36, 1.20)	(2.76, 0.66)	(5.13, 1.13)

ond column is the result obtained without inclusion of any three-body force. In the third and fourth columns a three-body interaction has been included in such a way that the energy of the computed resonances is moved down to the experimental values given in [39] ( $(E_R, \Gamma) = (0.89, 0.11)$  MeV and  $(E_R, \Gamma) = (2.03, 0.09)$  MeV) and in [40].

As we can immediately observe, once the energy of the resonances has been fitted to the experimental values, the corresponding widths are systematically bigger than the experimental ones. This comparatively much larger theoretical width suggests that more than half of the structure of the resonances is beyond the structure of an inert core and two surrounding neutrons.

Also, the computed  $0^+$  and  $1^-$  states could both correspond to the two states known experimentally. With the help of an attractive three-body force the energy of the two resonances can be fitted either to 0.9 MeV or 2.0 MeV (for the  $0^+$  case the energy of 2.0 MeV is ob-

tained without three-body force). It is then difficult from the calculation to determine which of the two resonances corresponds to the  $0^+$  state and which to the  $1^-$  state. However, since the calculation without three-body force naturally places the  $0^+$  state lower than the  $1^-$  state, one could think that the lower resonance at 0.9 MeV is more likely of  $0^+$  character, and the one at 2.0 MeV of  $1^-$  character, although the opposite can certainly not be excluded.

In any case, from the calculation we can exclude the quantum numbers  $2^+$  for the resonance at 0.9 MeV. Even for the lowest computed  $2^+$  it is not easy to reach the energy of 2.0 MeV, and an energy of 2.7 MeV is the lowest we can get. This is interesting because in Ref.[39] they suggest spin and parity  $2^+$  for the resonance at 0.9 MeV, and  $2^+$ ,  $3^-$ , or  $4^+$  for the one at 2.0 MeV.

Finally, the  $0^-$  state, unless missed in the searches for bound states, can only appear either as a virtual state or a very broad resonance structure.

#### IV. RESONANCE STRUCTURES

The structure of the resonance wave functions is reflected in the decomposition into partial waves of the two-body subsystems. The interest here is two-fold, that is bulk structure and asymptotic large-distance configurations. The bulk structure reflects where the largest probability is found, which has to be at relatively small distances since the wave function in the rotated frame vanishes exponentially at large distance as a bound state. In an intuitive picture of a reaction populating such a resonance, this short-distance large-probability part would be essential for the population cross section. On the other hand, the large-distance properties reveal which decay channel is preferred and in general give the branching ratios of these decay modes.

##### A. Partial waves of Bulk structure

We begin with the bulk structure of the partial-wave decomposed resonance wave function. We show in table II the probabilities of finding different configurations within the  $1^-$  resonance. The energy is adjusted with the three-body potential to be 0.89 MeV. The partial-wave decompositions do not change substantially by increasing this energy up to 2.0 MeV. The dominating configurations are total orbital angular momentum  $L = 1, 2$ . The  $L = 1$  ( $2$ ) configuration is with either  $p$  or  $s$  ( $d$ )-waves between the two neutrons, combined respectively with  $s$  ( $d$ ) or  $p$ -waves of their center of mass around the core. The Pauli principle then determines the spin combinations producing either 0 or 1. Expressing the same wave function in the other Jacobi system we find four comparable components with neutron-core in  $p$  or  $d$  combined with  $d$  or  $p$  partial waves of the last neutron around the neutron-core center of mass.

TABLE II. Components and weight of each component in the  $1^-$  resonance wave function (normalized to 1 in the complex scaling sense). The energy is chosen to be 0.89 MeV. The upper part is the first Jacobi set ( $x$  coordinate from neutron to neutron), and the lower part corresponds to the second and third Jacobi sets ( $x$  coordinate from core to neutron). Only the components contributing by at least by 1% are included. The orbital angular momenta are denoted by  $\ell_x$  (between two of the particles) and  $\ell_y$  (between the third particle and the center of mass of the other two particles). They couple to  $L$ . Correspondingly are the spins denoted  $s_x, s_y$  (the spin of the third particle, not given here) and the total spin,  $S$ , obtained by coupling. The value of  $K_{max}$  gives the maximum value for the hypermomentum [41] employed for this component. The probability in % is in the last column, and it is denoted as weight.

$\ell_x$	$\ell_y$	$L$	$s_x$	$S$	$K_{max}$	Weight (%)
0	1	1	0	0	300	29.7
1	0	1	1	1	200	10.8
1	2	1	1	1	160	1.5
1	2	2	1	1	300	34.3
2	1	1	0	0	200	6.8
2	3	1	0	0	60	3.2
3	2	1	1	1	60	1.7
3	2	2	1	1	60	5.6
3	4	2	1	1	40	4.9
4	3	2	0	0	40	1.0
0	1	1	1/2	1	160	1.1
1	2	1	1/2	0	200	18.4
1	2	1	1/2	1	120	6.4
1	2	2	1/2	1	300	20.9
2	1	1	1/2	0	300	20.3
2	1	1	1/2	1	200	6.2
2	1	2	1/2	1	300	25.1

TABLE III. Components and weight of each component in the  $0^+$  resonance wave function at 0.89 MeV. The notation is as in table II.

$\ell_x$	$\ell_y$	$L$	$s_x$	$S$	$K_{max}$	Weight (%)
0	0	0	0	0	240	61.6
1	1	1	1	1	240	28.3
2	2	0	0	0	200	10.1
0	0	0	1/2	0	100	3.2
1	1	0	1/2	0	100	1.4
1	1	1	1/2	1	100	5.6
2	2	0	1/2	0	200	65.0
2	2	1	1/2	1	200	24.8

TABLE IV. Components and weight of each component in the  $2^+$  resonance wave function at 5.36 MeV. The notation is as in table II.

$\ell_x$	$\ell_y$	$L$	$s_x$	$S$	$K_{max}$	Weight (%)
0	2	2	0	0	350	11.6
1	1	1	1	1	450	32.5
1	1	2	1	1	100	1.8
1	3	2	1	1	100	2.6
2	0	2	0	0	350	7.9
2	2	2	0	0	350	18.8
2	4	2	0	0	100	1.5
3	1	2	1	1	100	2.9
3	3	1	1	1	100	8.7
3	3	2	1	1	100	5.9
4	4	2	0	0	100	4.2
1	1	1	1/2	1	200	1.1
2	0	2	1/2	0	500	1.1
2	2	1	1/2	1	500	36.6
2	2	2	1/2	0	500	43.1
2	2	2	1/2	1	300	15.6

The  $0^+$  resonance is also a suitable candidate for both the two lowest-lying observed resonances. We show in table III its bulk structure for an energy of 0.89 MeV. The weights of these configurations would only change very little by increasing the energy to about 2.0 MeV. The two neutrons are in relative  $s$ ,  $p$ , or  $d$  waves and strongly decreasing probability with orbital angular momentum. This corresponds to the neutron-core essentially entirely in  $d$ -waves combined with the last neutron in  $d$ -waves.

The  $2^+$  resonance is not a natural candidate for the lowest resonance at 0.89 but very suitable for a high-lying resonance at about 5 MeV, and may be also for the 2.03 MeV resonance. We show in table IV its bulk structure for an energy of 5.4 MeV. The weights of these configurations are rather insensitive to variations of the energy by several MeV. The two neutrons are, as for  $0^+$ , in relative  $s$ ,  $p$ , or  $d$  waves but now the largest probability is for  $p$ -waves. The last neutron is correspondingly in  $d$ ,  $p$ , or  $s$  waves. In the other Jacobi system this corresponds to the neutron-core essentially entirely in  $d$ -waves combined with the last neutron in  $d$ -waves around this structure of the  $^{11}\text{Be}$  system.

The last of the appropriate quantum numbers is  $0^-$  which disappears into the continuum as soon as it is attempted lifted a little above the energy of the  $^{11}\text{Be}$  ground state. It is not possible to place such a resonance structure closer to the threshold of the excited state of  $^{11}\text{Be}$ , and much less in the true three-body continuum of  $^{12}\text{Be}$ . When the  $0^-$  state is genuinely bound, with a binding energy of about  $-1$  MeV, its bulk structure is given by table V of Ref.[27]. This structure does not change very much with the binding energy, and its main

TABLE V. Components and weight of each component in the  $0^-$  bound state wave function with an energy of  $-0.518$  MeV, slightly more bound than the  $-0.504$  MeV corresponding to the lowest one-body threshold, i.e. the  $1/2^+$  ground state of  $^{11}\text{Be}$ . The notation is as in table II.

$\ell_x$	$\ell_y$	$L$	$s_x$	$S$	$K_{max}$	Weight (%)
1	0	1	1	1	500	82.8
1	2	1	1	1	400	3.7
3	2	1	1	1	200	8.9
3	4	1	1	1	100	2.1
5	4	1	1	1	40	1.0
0	1	1	1/2	1	500	54.4
1	0	1	1/2	1	500	44.4

TABLE VI. Components and weight of each component in the  $0^-$  resonance wave function with an energy of  $-0.479$  MeV, which is just above the  $-0.504$  MeV corresponding to the lowest one-body threshold, i.e. the  $1/2^+$  ground state of  $^{11}\text{Be}$ . The notation is as in table II.

$\ell_x$	$\ell_y$	$L$	$s_x$	$S$	$K_{max}$	Weight (%)
1	0	1	1	1	500	9.2
1	2	1	1	1	400	12.7
3	2	1	1	1	200	14.7
3	4	1	1	1	200	13.5
5	4	1	1	1	100	12.6
5	6	1	1	1	100	10.4
7	6	1	1	1	60	9.0
7	8	1	1	1	40	7.1
9	8	1	1	1	40	6.0
9	10	1	1	1	40	4.7
0	1	1	1/2	1	500	55.5
1	0	1	1/2	1	500	25.3
1	2	1	1/2	1	400	2.4
2	1	1	1/2	1	400	10.4
2	3	1	1/2	1	200	1.0
3	2	1	1/2	1	200	3.5

characteristics are similar to the ones found when the system is made to be bound, but just below the  $-0.504$  MeV corresponding to the lowest one-body threshold, i.e. the  $1/2^+$  ground state of  $^{11}\text{Be}$ . This is shown in table V for a three-body energy of  $-0.518$  MeV. As in Ref.[27], the two neutrons in  $p$ -waves dominates with the core in an  $s$ -wave. The neutron-core structure is roughly equally distributed in  $s$  and  $p$ -waves with  $p$  and  $s$  partial waves for the last neutron in the motion around this  $^{11}\text{Be}$  state.

However, when increasing the energy of the  $0^-$  bound state, and lifting it above the  $^{11}\text{Be}$  ground state threshold, the partial wave decomposition changes. We show in table VI the results for a three-body energy of  $-0.479$

MeV. The neutron-neutron  $p$ -wave is now distributed over many components of higher relative angular momenta with correspondingly higher center of mass angular momenta around the core. In the second Jacobi system we find that the neutron-core  $s$ -wave component basically remains unchanged whereas the  $p$ -wave becomes distributed over many partial waves. Therefore, above the threshold the configuration is about 50% of the neutron- $^{10}\text{Be}$  in the ground state of  $^{11}\text{Be}$ . The other half of the probability is distributed among many partial waves. This fact strongly suggests that this part of the resonance structure approaches a free plane wave solution. Thus, the  $0^-$  structure above the  $^{11}\text{Be}$  ground state threshold resembles a coherent combination of a two-body structure, neutron- $^{11}\text{Be}(1/2^+)$ , and a three-body continuum state without resonance structure.

The energy ordered sequence of resonances is then most consistently in the model given by  $0^+$ ,  $1^-$ , and  $2^+$ , while  $0^-$  (unless missed in the searches for bound states) only appears as an attractive potential related to a virtual state.

### B. Spatial properties of the resonances

Resonances are quasi-stable systems produced by the presence of some potential barrier that keeps the particles close to each other for a certain amount of time. Eventually the particles tunnel through the barrier and the resonance decays. Even if this fact implies a non-square integrable wave function for the system, it is reasonable to ask ourselves about the spatial distribution of the resonance constituents while kept together inside the potential pocket. This analysis can be easily made through the complex scaled resonance wave function. In this way, we get rid of the divergent part of the wave function, which is associated to the spatial distribution after decay, while the structure of the inner part is maintained.

In particular, we shall construct the spatial distribution function by integrating the square of the wave function with respect to the directions of the  $\mathbf{x}$  and  $\mathbf{y}$  Jacobi coordinates. More precisely, we define it as:

$$D(J^\pi; r_x, r_y) = \int r_x^2 r_y^2 (\Psi^{J^\pi}(\mathbf{r}_x, \mathbf{r}_y))^2 d\Omega_x d\Omega_y, \quad (1)$$

where  $r_x$  is the distance between the two particles connected by the Jacobi coordinate  $\mathbf{x}$ , and  $r_y$  is the distance between the third particle and the center of mass of the first two. Obviously, for a system like  $^{12}\text{Be}$ , with a core and two neutrons, we can construct two spatial distribution functions, since  $r_x$  can refer either to the distance between the two neutrons or to the distance between one of the neutrons and the core.

It is important to note that the wave function  $\Psi^{J^\pi}$  is complex, and therefore the spatial distribution function  $D$  is complex as well (the square of the wave function is not the square of the modulus [44]). However, as discussed in [44], the imaginary part of the computed

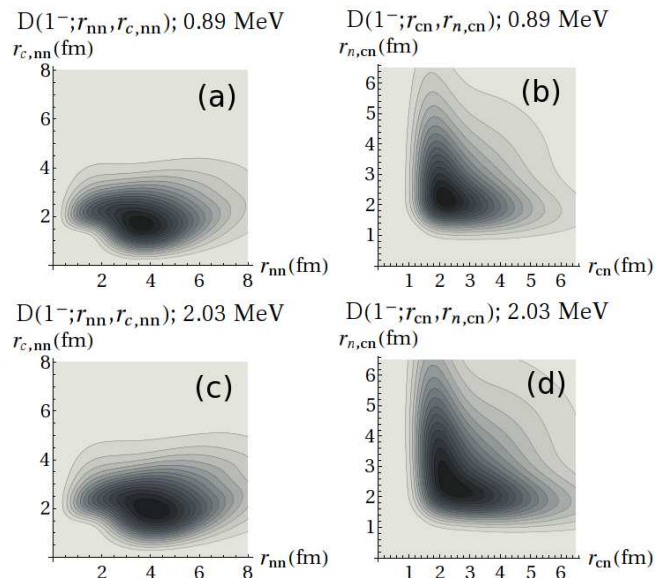


FIG. 6. (Color online) Contour plot of the spatial distribution function in Eq.(1) for the  $1^-$  resonance in  $^{12}\text{Be}$  when placed at 0.89 MeV (upper part), and when placed at 2.03 MeV (lower part). The figures on the left correspond to the first Jacobi set ( $r_x = r_{nn}$  is the distance between the two neutrons), and the figures on the right correspond to the second and third Jacobi sets ( $r_x = r_{cn}$  is the distance between one of the neutrons and the  $^{10}\text{Be}$  core). The darker the color in the plot the higher the value of the distribution function.

observables can be interpreted as the uncertainty of the measuring computed observable, while the real part is associated to the value of the observable itself (this is what happens for instance with the expectation value of the hamiltonian, which is the complex energy of the resonance). For this reason, we shall in the future consider only the real part of the distribution function  $D$  defined in Eq.(1).

Concerning the  $1^-$  states, the bound state is mainly built on the lowest and broadest adiabatic potential in Fig.1. This potential does not show any barrier, and therefore it can not be responsible for the appearance of  $1^-$  resonances. This is not happening with the second attractive potential, which together with the potential pocket exhibits as well a barrier providing the stability necessary for a finite width. This is in fact the potential responsible for the appearance of the  $1^-$  resonance whether it is placed at 0.89 or at 2.03 MeV.

Making use now of Eq.(1) we can investigate the spatial distribution of the two neutrons and the  $^{10}\text{Be}$  core in the  $1^-$  resonance. This is done in Fig. 6, where we show the contour plot of the spatial distribution function for the two resonance energies considered in this work. In the left part of the figure we give the results in the first Jacobi set, where the horizontal and vertical axes represent the distance between the two neutrons ( $r_{nn}$ ) and the distance between the core and the center of mass of the



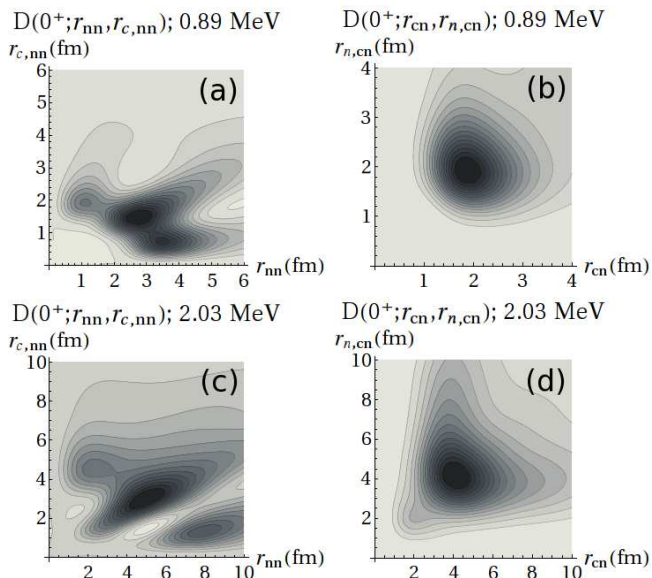


FIG. 7. (Color online) The same as Fig. 6 for the  $0^+$  resonance in  $^{12}\text{Be}$  when placed at 0.89 MeV (upper part), and when placed at 2.03 MeV (lower part).

two neutrons ( $r_{c,nn}$ ), respectively. In the right part of figure the second and third Jacobi sets are used, meaning that the coordinates used are the distance between the core and one of the neutrons ( $r_{cn}$ ), and the distance between the second neutron and the center of mass of the  $n-^{10}\text{Be}$  system ( $r_{n,cn}$ ). Obviously, a darker color in the figure implies a higher value of the distribution  $D$ .

As we can see, there are no relevant differences between the spatial structure depending on the energy. The increase in energy from about 1 MeV to about 2 MeV only moves very little the maxima in the figure towards bigger separation between particles, but the structure of the system remains the same. In the two cases shown, with energies 0.89 MeV (upper part) and 2.03 MeV (lower part), the system shows a clean maximum for the two neutrons about 4 fm far apart from each other, and the core about 2 fm from the center of mass of the two neutrons. This is essentially an isosceles triangle with the two neutrons defining the different side ( $\sim 4$  fm long), while the two other sides are about 2.7 fm long, which corresponds to the distance between the core and each of the two neutrons. This geometry is consistent with the distribution seen in the right part of the figure, where the maximum is found for  $r_{cn} \approx 2.6 - 2.7$  fm (due to the large mass of the core compared to the neutron mass we have that  $r_{n,cn} \approx r_{cn}$ ).

The  $0^+$  structures are found in two bound as well as in one resonance state. The bound states are built on the two attractive adiabatic potentials in Fig.1 without any barrier, see [27]. The  $0^+$  resonance is related to the other two attractive potentials in Fig.1, both of them showing a barrier. The relative weight for the energy of 0.89 MeV

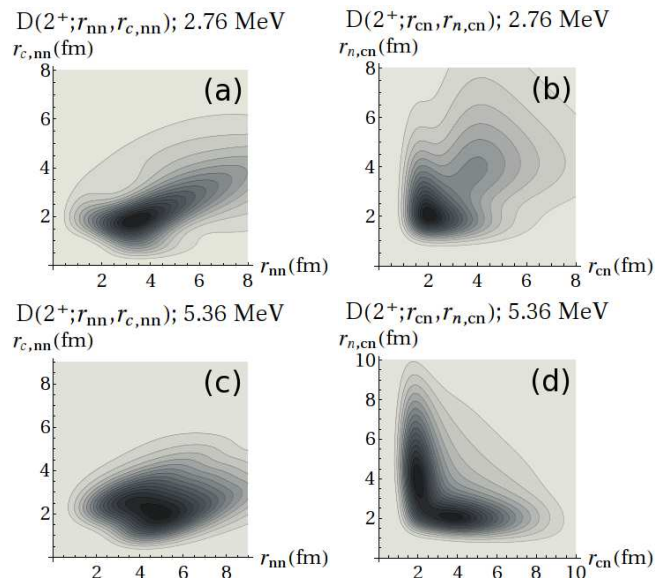


FIG. 8. (Color online) The same as Fig. 6 for the  $2^+$  resonance in  $^{12}\text{Be}$  when placed at 2.76 MeV (upper part), and when placed at 5.36 MeV (lower part).

is 66% on the deepest and narrowest potential and the remaining 44% is from the high-lying attractive potential with a barrier. Increasing the energy to 2.03 MeV, the latter high-lying potential becomes responsible for 92% whereas the remaining 8% is shared among the many other potentials. The structure has changed substantially away from that of the deep and narrow potential.

The spatial distribution for the  $0^+$  resonance is shown in Fig. 7. In this case the jump from 0.89 MeV to 2.03 MeV increases the separation between particles more significantly than for the  $1^-$  resonance. The maximum of the distribution appears for a distance between neutrons smaller than 3 fm when the energy is 0.89 MeV (upper part), and about 5 fm when the energy is 2.03 MeV (lower part). In any case, the spatial distribution is similar (but scaled) in both cases. In fact, in both cases we observe two additional maxima corresponding to an almost aligned distribution with the  $^{10}\text{Be}$  core very close to the center of mass of the two neutrons, an another corresponding to a dineutron (the two neutrons close to each other) and the core far apart.

The  $2^+$  structure is also found as a bound state which is predominantly built on the lowest attractive adiabatic potential. The additional  $2^+$  resonance structure which occurs “naturally” without a three-body potential at 5.36 MeV is almost entirely built on the second potential with an attractive pocket at small distance. Moving this resonance down with an attractive three-body potential increases the contribution from the potential with the attractive pocket at about 5 fm in Fig.1. For an energy of 2.77 MeV these two potentials share roughly equally the probabilities.

The spatial distribution function for the  $2^+$  resonance is shown in Fig. 8. Contrary to what happened in the  $1^-$  and  $2^+$  cases, where the energy change between the two cases shown was relatively small, now the energy variation is bigger (from 2.76 MeV to 5.36 MeV), and the upper and lower parts in the figure show clear differences. This is more easily seen in the second and third Jacobi sets (right part of the figure). When the energy is chosen to be 2.76 MeV the two neutrons like more to be equally separated from the core (a bit more than 2 fm), but for an energy of 5.36 MeV a structure with a neutron close to the core (about 2 fm) and the second one far from it (around 4.5 fm) is preferred.

## V. DECAY AND PRODUCTION OF $^{12}\text{Be}$

The calculated structures can be used to determine both the probability of the different decay modes and the probability of populating a resonance. Both the population and decay of the resonances in  $^{12}\text{Be}$  can be studied experimentally. The two quantities are very dependent on the quantum numbers of the resonances, hence a comparison between the theoretically calculated and the experimentally determined strength can be used to assign quantum numbers for the resonances.

### A. Decay modes

The decay channels are determined from the large-distance structure of the radial wave functions. As seen in Fig.1, each adiabatic potential corresponds to a very specific asymptotic configuration, i.e., bound  $^{11}\text{Be}$  (either in the ground state or in the excited state) plus a neutron,  $^{11}\text{Be}$  populating a two-body resonance plus a neutron, or the three constituents in the continuum. This is because the observable final state momenta of each of the emerging particles precisely are reflected in the coordinate wave function at asymptotic large distances [8, 45]. The probability of decaying through a given channel is then the probability of occupying the adiabatic potential describing that channel at large distance.

The angular momenta and parities of the experimentally observed resonances are not known, although in some cases their values are suggested as the most likely according to the experimental conditions. The energies chosen for each of the resonances computed in this work meet these conditions, and we therefore calculate branching ratios for the  $0^+$ ,  $1^-$ , and  $2^+$  resonances each of them placed at two different energies. The computed branching ratios for each of them are given in table VII, where the energy and width of each resonance ( $E, \Gamma$ ) is given in MeV. The decay channels denoted by “ $\frac{1}{2}^+ + n$ ” and “ $\frac{1}{2}^- + n$ ” represent emission of one neutron plus  $^{11}\text{Be}$  either in the ground state or in its bound excited state. The direct decay into the three-body continuum, with

TABLE VII. Branching ratios (in %) after decay of the resonance with angular momentum and parity  $J^\pi$ . The resonance energies and widths,  $E$  and  $\Gamma$ , are given in MeV. For each decay channel we specify the half-integer angular momentum of  $^{11}\text{Be}$  or the  $0^+$  angular momentum of  $^{10}\text{Be}$ , and where each  $n$  indicates emission of one neutron.

$J^\pi$	$(E, \Gamma)$	$\frac{1}{2}^+ + n$	$\frac{1}{2}^- + n$	$0^+ + n + n$	$\frac{3}{2}^+ + n$	$\frac{5}{2}^+ + n$
$0^+$	(0.89,0.32)	8.6	59.5	31.8	0.0	0.0
$0^+$	(2.03,0.84)	0.8	12.8	48.4	0.0	38.0
$1^-$	(0.89,0.22)	17.4	74.5	8.1	0.0	0.0
$1^-$	(2.03,0.50)	6.3	84.5	7.7	0.0	1.5
$2^+$	(2.76,0.66)	14.9	0.9	65.2	0.0	19.0
$2^+$	(5.36,1.20)	8.2	1.8	55.5	13.9	20.6

the  $^{10}\text{Be}$  core in the  $0^+$  ground state, is denoted by “ $0^+ + n + n$ ”. Finally, “ $\frac{3}{2}^+ + n$ ” and “ $\frac{5}{2}^+ + n$ ” correspond to sequential decay through the  $\frac{3}{2}^+$  and  $\frac{5}{2}^+$  resonances in  $^{11}\text{Be}$ , which eventually decay into the two-body continuum of  $^{10}\text{Be}$  and a neutron.

For  $0^+$  resonance at  $E = 0.89$  MeV the preferred decay channels are either one-neutron decay to the excited  $1/2^-$  state of  $^{11}\text{Be}$  or direct decay to the three-body continuum. Only about 8.6% of the decay takes place through the ground state of  $^{11}\text{Be}$ . For the higher energy of  $E = 2.03$  MeV, since the energy of the  $5/2^+$  resonance in  $^{11}\text{Be}$  is 1.28 MeV, the probability for sequential decay through this resonance now becomes prominent. The direct decay is also increased at the expense of the one-neutron decay branch, that reduces from about 58% to about 14%, and where in particular the decay through the ground state of  $^{11}\text{Be}$  almost disappears.

If the lowest resonance at about 0.9 MeV is a  $1^-$  state, we find that most decays proceed by one-neutron emission to the excited  $^{11}\text{Be}$  state and a smaller but significant fraction decays to the  $^{11}\text{Be}$  ground state. The direct decay into the continuum amounts only to about 8%. If the  $1^-$  state is at about 2 MeV the branching ratios are even larger for decay into the excited  $^{11}\text{Be}$  state and less than 10% into the ground state, while the direct decay remains around 8%.

The lowest resonance have been seen in a  $d(^{11}\text{Be}, p)^{12}\text{Be}$  experiment at ISOLDE, by gating on the gamma from the sequential decay through the  $1/2^-$  bound state in  $^{11}\text{Be}$  [46]. This is the first experiment in which a given decay channel from a resonance in  $^{12}\text{Be}$  has been singled out, and could open up for branching ratio measurement, but the analysis is still ongoing. A measurement of the branching ratio will give a strong indication of the quantum numbers of the resonances. As we can see, the  $^{12}\text{Be}$  resonance at about 0.9 MeV and the one about 2.0 MeV would have rather different decay branching ratios depending on which of them is the  $0^+$  state and which the  $1^-$  state. A  $0^+$  state would decay with a large component of direct decay

into the continuum. This component reduces drastically in the case of the  $1^-$  resonance, that clearly prefers to decay through the  $1/2^-$  state in  $^{11}\text{Be}$ .

The calculated  $2^+$  resonance is naturally placed at a higher energy, or alternatively predominantly of a non-three body structure. For an energy of 5.36 MeV the dominating decay channel is direct decay or sequential decays through either  $3/2^+$  or  $5/2^+$  resonances in  $^{11}\text{Be}$ . For a lower energy of 2.76 MeV the direct decay is even more dominating, while decay to the ground state has increased at the expense of the sequential decay through the high-lying  $3/2^+$  resonance, which for energy reasons disappears (the energy of  $3/2^+$  resonance in  $^{11}\text{Be}$  is 2.90 MeV).

### B. Production strength

While the decay of the resonances of  $^{12}\text{Be}$  are still to be measured, the continuum of  $^{12}\text{Be}$  has been probed in both neutron transfer and charge exchange experiments. So far only two experiments have been able to clearly identify any resonances [39, 40], and the information is limited to excitation energy and width. Both experiments show clear resonances at 0.89 MeV and 2.03 MeV, and tentatively quantum numbers of  $2^+$  and  $0^+$  or  $4^+$  is suggested from DWBA calculations. A large peak at 5.13 MeV seen in the  $^9\text{Be}(^{12}\text{C}, ^9\text{C})^{12}\text{Be}$  experiment [40] strongly indicates of a third resonance. Unfortunately this resonance cannot be confirmed by the  $^{10}\text{Be}(t,p)^{12}\text{Be}$  reaction [39] due to limits in the energy range. A resonance at 5.13 MeV would be a good candidate for the predicted  $2^+$ .

The probability of populating a resonance in a transfer reaction is dependent on the overlap between the total wave function of the resonance and the configuration probed by the reaction. Take (t,p) as an example, assuming a direct reaction, the two-neutrons from a relative  $s$ -state in the triton would prefer an  $s$ -wave in the first Jacobi system. Comparing this configuration with the total wave function can be done by looking at the weights in tables II-IV. Here  $0^+$  is dominated by  $s$ -wave of 60%, twice as large as  $1^-$  with 30% while  $2^+$  is reduced by an additional factor of 3 to about 12%. This indicates a larger probability of probing a  $0^+$  than a  $1^-$  and especially a  $2^+$  resonance in a (t,p) reaction. These weights have been calculated for the bound states by Romero-Redondo et al [27] to be 90%, 37%, 46% for  $0_1^+$ ,  $2^+$ ,  $1^-$  states. The weights predict a stronger population of the  $0^+$  ground state and the bound  $2^+$  than the population of the bound  $1^-$ . These findings are consistent with the (t,p) measurement of Fortune, [39]. The strong population of the two resonances in the experiment is then not favored by the suggested  $2^+$  structure, which indicate only very weak population. The suggested quantum numbers of  $0^+$  for the lowest resonance and  $1^-$  for the second is more consistent with the large population of especially the lowest resonance.

Sequential transfers through  $^{11}\text{Be}$  could also occur, and distort the picture. Whether the reaction is direct or sequential cannot be distinguished experimentally, but information from a (d,p) reaction might be helpful. A similar comparison can be made for a (d,p) reaction. Again assuming the simplest possible reaction, adding one neutron to the ground state of  $^{11}\text{Be}$ . In this case all weights are around 1%, which indicates that contributions from higher order reactions would be competitive. In fact for all three sets of quantum numbers ( $0^+$ ,  $1^-$ ,  $2^+$ ) an excitation to the  $d$ -shell is required to get more than 10% weight, hence coupling to these continuum states should be taken into account in any reaction calculation. This is supported by a scattering experiment with  $^{11}\text{Be}$  on  $^{64}\text{Zn}$  which shows a large break up channel for  $^{11}\text{Be}$  [47].

A (d,p) reaction could also be used to populate the predicted  $0^-$  state around the one neutron threshold, as the reaction does not favor natural parity states. Comparing the strengths for the simplest reactions to populate a  $0^-$  from a (t,p) and (d,p) reaction respectively can be done by comparing the weights in tab VI. Here the weights for the (t,p) is less than 1% while it is 55% for a (d,p). Therefore a population in a (t,p) should be very weak, nonetheless an indication of a broad weakly populated resonance at  $-0.3$  MeV is seen in the (t,p) reaction by Fortune, [39]. The peak is to very weak, but if it is indeed a resonance, it should be populated and seen in a (d,p) measurement.

Further improved experimental investigations would help to test the validity of the model interpretation. This includes measurements of both population and decay of the channels.

## VI. SUMMARY AND CONCLUSIONS

We employ the technique of hyperspherical adiabatic expansion method combined with complex coordinate scaling. We investigate the continuum states, mostly resonances, of  $^{12}\text{Be}$  in a three-body model where the constituents are two neutrons and  $^{10}\text{Be}$ . The previously known four bound states are fairly well described in such a model. This therefore already determines a successful set of two-body interactions, which are now used in an extension to study low-lying continuum states above the three-body breakup threshold.

The most probable angular momenta and parities are  $0^\pm$ ,  $1^-$  and  $2^+$ . We first compute a series of the lowest adiabatic potentials with these quantum numbers. They exhibit lots of structure and several potentials have attractive regions at small distance. This already indicates possible bound states or resonances with corresponding properties. The energies are in principle found as solutions to the hyperradial equations but the three-body model cannot be expected to provide precise energies. Therefore we fine-tune with a three-body potential which moves the bound states/resonances up or down. The widths of the resonances are then correlated with

the resonance position. We should here remember that our computed width should be larger than the measured value because we only have the three-body component in the model. Any additional components would tend to reduce the computed width.

The naturally occurring lowest of these states is the  $0^-$  bound state. So far it has not been found experimentally and perhaps it instead is pushed up above the one- or perhaps even the two-neutron threshold. In attempts to move the energy from a bound to an unbound state, we find that the width increases dramatically just above the lowest one-neutron emission threshold. The structure of the state then corresponds to a coherent combination of  $^{11}\text{Be}$  in the ground state surrounded by one neutron and a genuine three-body structure. Quickly it becomes impossible to trace the resonance which could turn into either a virtual state or a very broad neutron- $^{11}\text{Be}$  resonance.

Both  $1^-$  and  $0^+$  resonances can rather easily be placed at the positions of the two lowest resonances at about 0.9 MeV and 2.0 MeV above the three-body threshold. It is then natural to associate these quantum numbers with these resonances. The width comparison to measured values suggest that  $0^+$  is the lowest state at about 0.89 MeV and  $1^-$  is at 2.03 MeV, but the opposite can not be excluded. The  $2^+$  state also appears as a resonance but it requires a very strong three-body attraction to pull it down to these low energies. It is then natural to associate this state with a higher-lying resonance at about 5.36 MeV.

We calculate the structure of these resonances expressed as partial-wave decomposed configurations. The neutron-neutron relative wave functions are mixtures of  $s$ ,  $p$ , and  $d$ -waves whereas the neutron- $^{11}\text{Be}$  relative wave functions consists of essentially only  $d$ -waves for the  $0^+$  and  $2^+$  resonances, and both  $p$  and  $d$ -waves for the  $1^-$  resonance.

The assignment of quantum numbers requires addi-

tional information. The lowest-lying resonances have for some time tentatively been assigned to  $2^+$ . The present model rather suggest  $1^-$  and  $0^+$ . To find further evidence we calculate the branching ratios for decays into different channels. These quantities are observables and could help to confirm assignments of angular momentum and parity. We find several coexisting decay channels for all three resonances depending on which energy position is chosen. Channels like one-neutron, three-body direct as well as three-body sequential via different  $^{11}\text{Be}$  resonances are all possible.

The detailed comparison to measured results must unfortunately include calculations of transfer cross sections. This would provide information about population of the resonances which in combination with our branching ratios could distinguish between different angular momentum and parity assignments.

In summary, we have calculated the low-lying three-body resonance structure of  $^{12}\text{Be}$ . Partial wave decomposition for small as well as large distances are now available for this model. We find surprisingly many different resonances and bound states for such a light neutron dripline nucleus. The computed structures can now be compared to measurements. Our results and the available data are all consistent with  $0^+$  at 0.89 MeV,  $1^-$  at 2.03 MeV and  $2^+$  at 5.13 MeV.

## ACKNOWLEDGMENTS

This problem was suggested by H. Fynbo and K. Riisager in connection with detailed analysis of experiments of neutron transfer from deuteron to  $^{11}\text{Be}$ . We appreciate the information from numerous discussions. This work was partly supported by funds provided by DGI of MINECO under contract No. FIS2008-01301.

- 
- [1] I. Tanihata, H. Hamagaki, O. Hashimoto, Y. Shida, N. Yoshikawa, K. Sugimoto, O. Yamakawa, T. Kobayashi, and N. Takahashi, *Phys. Rev. Lett.* **55** (1985) 2676.
  - [2] P.G. Hansen and B. Jonson, *Europhys. Lett.* **4** (1987) 409.
  - [3] M.V. Zhukov, B.V. Danilin, D.V. Fedorov, J.M. Bang, I.J. Thompson, and J.S. Vaagen, *Phys. Rep.* **231** (1993) 151.
  - [4] A.S. Jensen, K. Riisager, D.V. Fedorov, and E. Garrido, *Rev. Mod. Phys.* **76** (2004) 1.
  - [5] Y. Kanada-En'yo, *Phys. Rev. Lett.* **81** (1998) 5291.
  - [6] P. Descouvemont, *Nucl. Phys. A* **709** (2002) 275.
  - [7] T. Neff and H. Feldmeier, *Nucl. Phys. A* **738** (2004) 357.
  - [8] R. Álvarez-Rodríguez, A.S. Jensen, E. Garrido, D.V. Fedorov, and H.O.U. Fynbo, *Phys. Rev. C* **77** (2008) 064305.
  - [9] J. Görres, H. Herndl, I.J. Thompson, M. Wiescher, *Phys. Rev. C* **52** (1995) 2231.
  - [10] K. Sumiyoshi, H. Utsunomiya, S. Goko, and T. Kajino, *Nucl. Phys. A* **709** (2002) 467.
  - [11] F.C. Barker and H.O.U. Fynbo, *Nucl. Phys. A* **776** (2006) 52.
  - [12] R. Álvarez-Rodríguez, H.O.U. Fynbo, A.S. Jensen, and E. Garrido, *Phys. Rev. Lett.* **100** (2008) 192501.
  - [13] E. Garrido, D.V. Fedorov, and A.S. Jensen, *Phys. Lett. B* **684** (2010) 132.
  - [14] A. Csótó, *Phys. Rev. C* **49** (1994) 3035.
  - [15] V. Vasilevsky, A.V. Nesterov, F. Arickx, and J. Broeckhove, *Phys. Rev. C* **63** (2001) 034607.
  - [16] E. Garrido, D.V. Fedorov, H.O.U. Fynbo, and A.S. Jensen, *Nucl. Phys. A* **781** (2007) 387.
  - [17] P. Papka *et al.*, *Phys. Rev. C* **81** (2010) 054308.
  - [18] M. Zinser *et al.*, *Phys. Rev. Lett.* **75** (1995) 1719.
  - [19] E. Garrido, D.V. Fedorov, and A.S. Jensen, *Nucl. Phys. A* **700** (2002) 117.
  - [20] H.B. Jeppesen *et al.*, *Phys. Lett. B* **642** (2006) 449.

- [21] D.V. Fedorov, E. Garrido, and A.S. Jensen, Phys. Rev. C **51** (1995) 3052.
- [22] V. Guimarães *et al.*, Phys. Rev. C **58** (1998) 116.
- [23] E. Garrido, D.V. Fedorov, and A.S. Jensen, Nucl. Phys. A **733** (2004) 85.
- [24] T. Oishi, K. Hagino, and H. Sagawa, Phys. Rev. C **82** (2010) 024315.
- [25] T. Otsuka, N. Fukunishi, and H. Sagawa, Phys. Rev. Lett. **70** (1993) 1385.
- [26] F. Nunes, I.J. Thompson, R.C. Johnson, Nucl. Phys. A **596** (1996) 171.
- [27] C. Romero-Redondo, E. Garrido, D.V. Fedorov and A.S. Jensen, Phys. Rev. C **77** (2008) 054313.
- [28] M. Dufour, P. Descouvemont, and F. Nowacki, Nucl. Phys. A **836** (2010) 242.
- [29] R. Kanungo *et al.*, Phys. Lett. B **682** (2010) 391.
- [30] A.A. Korshennikov *et al.*, Phys. Rev. Lett. **78** (1997) 2317.
- [31] S. Kumar and V. S. Bhasin, Phys. Rev. C **65** (2002) 034007.
- [32] E. Garrido, D.V. Fedorov, and A.S. Jensen, Nucl. Phys. A **708** (2002) 277.
- [33] T. Nakamura *et al.*, Phys. Rev. Lett. **96** (2006) 252502.
- [34] P. Descouvemont, Phys. Rev. C **52** (1995) 704.
- [35] H. Simon *et al.*, Nucl. Phys. A **791** (2007) 267.
- [36] I. Talmi and I. Unna, Phys. Rev. Lett. **4** (1960) 469.
- [37] C. Romero-Redondo, E. Garrido, D.V. Fedorov and A.S. Jensen, Phys. Lett. B **660** (2008) 32.
- [38] G. Blanchon, N. Vinh Mau, A. Bonaccorso, M. Dupuis, and N. Pillet, Phys. Rev. C **82** (2010) 034313.
- [39] H.T. Fortune, G.-B. Liu, D.E. Alburger, Phys. Rev. C **50** (1994) 1355.
- [40] H. G. Bohlen *et al.*, int. J. Mod. Phys. E **17** (2008) 2067.
- [41] E. Nielsen, D.V. Fedorov, A.S. Jensen, E. Garrido, Phys. Rep. **347** (2001) 373.
- [42] D.V. Fedorov, E. Garrido, and A.S. Jensen, Few-body Syst. **33** (2003) 153.
- [43] N. Fukuda *et al.*, Phys. Rev. C **70** (2004) 054606.
- [44] N. Moiseyev, Phys. Rep. **302** (1998) 211.
- [45] R. Álvarez-Rodríguez, A.S. Jensen, D.V. Fedorov, H.O.U. Fynbo, and E. Garrido, Phys. Rev. Lett. **99** (2007) 072503.
- [46] J. Johansen, AIP. Conf. Proc. **1377** (2010) 368.
- [47] A. Di Pietro *et al.*, Phys. Rev. Lett. **105** (2010) 022701.